Macromolecules
ARTICLE

Macromolecules **2009**, *42*, 8899–8906 **8899**
DOI: 10.1021/ma901604m

Wideline Separation (WISE) NMR of Native Elastin

Kosuke Ohgo, Walter P. Niemczura, Taeko Muroi, Allen K. Onizuka, and Kristin K. Kumashiro*

Department of Chemistry, University of Hawaii, Honolulu, Hawaii 96822

Received July 21, 2009; Revised Manuscript Received October 7, 2009

ABSTRACT: Native elastin is an insoluble, amorphous (noncrystalline) protein with significant hydrophobic character. As its name suggests, the elasticity of blood vessels and other tissue types in vertebrates originates from this protein. We have previously shown that there is significant structural heterogeneity in this protein and its mimetics, and our earlier data indicated that its dynamic profile includes motions under multiple time scales. To examine this picture further, we use WIdeline SEparation (WISE) NMR experiments to characterize the natural-abundance ^{13}C populations of unenriched elastin in fully hydrated and lyophilized states. The hydrated elastin has only one peak in the indirect dimension, reflective of significant motional narrowing. In contrast, the lyophilized elastin has a broad feature, indicating limited or no motion. In addition, however, our results indicate that a faster motion is also present, even in the absence of the water. The details of the line fitting and the possible implications for elastin are discussed.

Introduction

Elasticity in vertebrate tissue originates from the protein *elastin*, an insoluble, cross-linked protein assembled from its high-molecular-weight water-soluble monomer *tropoelastin*.[1,2] Elastin is comprised of hydrophobic and cross-linking domains. The former has an abundance of repeating polypenta- and polyhexapeptide sequences, some of which are often defined as peptide mimetics of elasticity. The cross-linking domains typically contain alanine-rich sequences. The protein's overall composition is dominated by small amino acids with nonpolar residues, like glycine, proline, alanine, and valine. This largely hydrophobic composition and extensive nature of the protein make high-resolution studies by solution nuclear magnetic resonance (NMR) spectroscopy and X-ray crystallography intractable. As a result, the detailed picture of elastin's organization is only slowly emerging with solid-state NMR studies.[3−7]

Elastin's structure−function relationships have been the subject of great debate. Historically, elastin was often compared to natural rubbers and other hydrocarbon-based elastomers; i.e., this protein is completely unstructured, with restoration of fiber shape rooted in arguments that rely upon entropy.[8,9] Tamburro proposes a conformational equilibrium in elastin, of which the populations of various configurations change with stretching and contraction.[10] Recently, results from this lab and others indicate that the nature of heterogeneity in elastin is both structural and dynamic in nature.[5−7] However, details remain elusive, due largely to the extensive nature of this protein.

The WIdeline SEparation (WISE) NMR experiments were first used to characterize dynamics in synthetic organic polymers.[11,12] In this two-dimensional (2D) magic-angle-spinning (MAS) experiment, a ^1H 90° pulse is applied, followed by the t_1 evolution period. During t_1, the ^1H magnetization evolves under primarily $^1H-^1H$ and $^{13}C-^1H$ dipolar couplings. After this t_1 evolution period, magnetization exchange by cross-polarization occurs under Hartmann−Hahn (HH) match conditions, and ^{13}C detection then occurs. A useful variation of WISE utilizes ^{13}C decoupling applied during t_1,[13] so that the heteronuclear dipolar couplings are removed during the t_1 period. The widths of the proton line shapes in the indirectly detected dimension are then used as a quantitative measure of mobility in synthetic polymers and their biological counterparts. The dipolar WISE experiment has been applied to pursue questions in a range of systems, including natural rubbers[14,15] and spider silk in wet and dry states.[16,17]

It is noted that another variation of the dipolar WISE experiment uses Lee−Goldburg cross-polarization (LG-CP)[18,19] instead of the more "broadband" selection of HH-CP. Interestingly, the target system chosen for this LG-WISE experiment was the elastin mimetic based on the VPGXG (X = Gly or Lys) motif,[20] found in the hydrophobic domains of the native protein. Although the selectivity of LG-CP is advantageous, we find that HH-CP with decoupling during t_1 is a reasonably robust and easy-to-implement experiment, and it is well-suited for the present case.

Finally, "J-WISE", a variation of the solid-state heteronuclear single-quantum coherence (HSQC) experiment, has previously been used to detect proton line shapes via the J-couplings.[21] This elegant experiment, however, does not have the sensitivity required for our samples, which are not isotopically enriched. As a comparison, the 2D J-WISE experiment applied to a sample of onion cell wall material required 50 t_1 points of 8K scans apiece. With a 1 s recycle delay and quadrature detection in the indirect dimension, the entire experiment took over 10 days. The typical lyophilized elastin sample in the dipolar WISE required ~22 h, whereas the data set for the hydrated protein was acquired over 3 days for 1K scans per t_1 point due to its lowered CP transfer rates in the presence of water.[6] With the longer recycle delay and more scans, the application of J-WISE to elastin requires almost 1 month, which cannot be easily accommodated in most settings.

As noted in related studies,[6,22] the need for strategies that allow characterization of unlabeled elastin is as great as the ones for

*Corresponding author: Tel (808) 956-5733; Fax (808) 956-5908; e-mail kumashir@hawaii.edu.

Published on Web 10/26/2009

enriched samples. Briefly, the nature of elastin, collagen, and other fibrous proteins is such that uniform labeling is not as well-developed as with smaller proteins, which may be produced by solid-phase peptide synthesis. Bacterial expression of full-length tropoelastin has been accomplished,[23] but the NMR of the cross-linked recombinant material is only just underway. Hence, with the challenges of sample preparation for enriched elastin, it is essential to develop strategies to study this protein in natural abundance.

In the present study, we use dipolar WISE to characterize samples of lyophilized and hydrated elastin. The lyophilized protein has a two-component line shape which is best fit with one narrow and one broad line shape. The elastin is purified from tissue, so there is no isotopic enrichment. These experiments characterize the natural-abundance ^{13}C populations. The results are compared to previously published WISE studies of an elastin mimetic, supercontracted spider silk, and natural rubbers.

Experimental Section

Elastin samples were purified from bovine nuchal ligament using the cyanogen bromide treatment, as described previously.[6] Typical sample sizes were 22 and 60 mg for the lyophilized and hydrated elastin samples, respectively. The residual water content was determined by placing lyophilized elastin samples in a desiccator with P_2O_5 for 120 h at room temperature. The amount of the residual water in lyophilized elastin was 3−4 mass %. Glycine, L-alanine, and L-valine were used as purchased (Sigma-Aldrich, St. Louis, MO). Typical sample sizes of the amino acids were 54−55 mg.

Rotors were sealed with a top spacer fitted with fluorosilicone micro O-rings (Apple, Lancaster, NY).[24] O-ring seals are necessary to maintain the hydration level (60 mass % water) of hydrated elastin during data collection. Top and bottom spacers are machined from Kel-F for reduced ^{13}C background signal.

NMR data were acquired on a Varian Unity Inova WB 400 spectrometer, equipped with a 4 mm HXY-T3 MAS probe (Chemagnetics/Varian NMR, Fort Collins, CO). The spinning speeds used in MAS experiments were 6 and 8 kHz. Data were acquired at 37.0 °C. ^{13}C chemical shifts were referenced to the tetramethylsilane scale, using hexamethylbenzene as an external standard [$\delta(^{13}CH_3)$ = 17.0 ppm at 37 °C].

The pulse sequence for the dipolar WISE experiment is similar to the original version.[11] Briefly, a ^1H 90° pulse followed by the t_1 evolution period and then CP for ^{13}C detection. For broadband excitation of the ^1H populations, a 3.2 μs ^1H 90° pulse was followed by 200 μs or 1 ms contact times. Recycle delays were 5 and 4 s for the amino acids and elastin, respectively. A linear ramped-amplitude CP sequence[25] was used for protons to restore a broader matching profile. The average field strength of CP was $\gamma B_1/2\pi = 50$ kHz, with a linear ramp width of 9.5 kHz. The spectral width in the indirect dimension was 75 kHz for the hydrated sample. For the lyophilized sample, the spectral width was increased to 200 and 250 kHz for the 8 and 6 kHz spinning speeds, respectively. The spectral width of 250 kHz was applied for the amino acid samples. Thirty-two t_1 increments were used in the elastin experiments. Sixty-four t_1 increments were used in experiments for the amino acids. The States method was applied to obtain phase-sensitive 2D spectra. In this study, ^{13}C CW decoupling was applied during t_1 evolution to reduce the $^1H-^{13}C$ dipolar coupling.[13] The decoupling field strength for ^{13}C during t_1 was $\gamma B_1/2\pi = 50$ kHz. Typical applied ^1H field strengths for high-power TPPM decoupling[26] during acquisition were $\gamma B_1/2\pi$ = 78 kHz.

The two-component line shapes in the indirect dimension were best-fit with equations described previously by Emsley and co-workers.[21]

$$S(\omega) = S_1(\omega) + S_2(\omega) \tag{1}$$

$$S_1(\omega) = \sum_{i=-n}^{n} I_1 \exp\left\{ -4 \ln 2 \left[\left(\frac{n\omega_r}{\Delta_1} \right)^2 + \left(\frac{\omega - \omega_{01} - n\omega_r}{\lambda_1} \right)^2 \right] \right\} \tag{2}$$

$$S_2(\omega) = I_2 \exp\left\{ -4 \ln 2 \left(\frac{\omega - \omega_{02}}{\Delta_2} \right)^2 \right\} \tag{3}$$

The total signal $S(\omega)$ is a sum of a broader component $S_1(\omega)$ and a narrow contribution $S_2(\omega)$, with respective "intensities" I_1 and I_2. The $S_1(\omega)$ component has a Gaussian distribution of the spinning sidebands intensity. The $S_2(\omega)$ contribution is a Gaussian line shape without sidebands. The sample spinning rate is ω_r, and there are $n = 4$ sidebands. The line width of each sideband is given by λ_1. The center frequencies for each of the two components are ω_{01} and ω_{02}, which were set to the same value. Finally, the widths of the contributions are determined as Δ_1 and Δ_2. Prior to the fitting, the maximum height in each 2D spectrum was normalized to 1.0.

As an alternate model, the ^1H line shapes were fit with two overlapping spinning sideband patterns, as

$$S(\omega) = S_1(\omega) + S_1'(\omega) \tag{4}$$

in which both contributions are described by eq 2, i.e., one series for the $S_1(\omega)$ and another for $S_1'(\omega)$, to obtain the intensities I_1 and I_1', line widths Δ_1 and Δ_1', and line widths of the sidebands λ_1 and λ_1'. The center frequencies ω_{01} and ω_{01}' were set to the same value for most of the analyses. The exception was the fit of the ^1H slice of Cα-Gly with 200 μs contact time in the lyophilized sample, with different center frequencies ω_{01} and ω_{01}'.

The nonlinear line fitting was done by the simplex search method using MATLAB (MathWorks Inc., Natick, MA).

Root-mean-square-deviation (rmsd) values between observed, and calculated ^1H line shapes were evaluated, with the definition

$$\text{rmsd} = \sqrt{\frac{\sum_{i=1}^{N} [S_i^{\text{obsd}} - S_i^{\text{calc}}]^2}{N}} \tag{5}$$

where S_i^{obsd} and S_i^{calc} are the observed and calculated data points, respectively, over the $i = 1$ to N points in the frequency domain in the indirect dimension and $N = 1024$ in this analysis.

The order parameter S_{HH} for each of the resolved sites was calculated from the widths of the broad components in the indirect dimension line shape for the single amino acid and its corresponding peak in elastin.

$$S_{HH} = \frac{\Delta_1^{\text{elastin}}}{\Delta_1^{\text{amino acid}}} \tag{6}$$

Results and Discussion

1. WISE of the Lyophilized Elastin Indicates the Presence of Two Distinguishable Populations. Previous studies used 1D CPMAS NMR experiments to characterize the natural-abundance ^{13}C populations of lyophilized and hydrated elastin from bovine nuchal ligament.[6] Briefly, the spectrum of the lyophilized elastin sample includes a broad and relatively featureless backbone carbonyl resonance centered

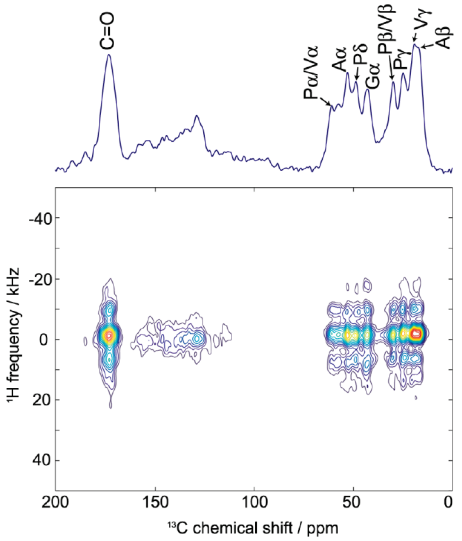

Figure 1. $^{1}H-^{13}C$ 2D WISE spectrum of lyophilized elastin with 1 ms contact time and 8 kHz MAS. Skyline projection along the ^{13}C dimension is also shown.

at 172 ppm, a broad and weaker peak at 130 ppm for the aromatic side chain carbons, plus 8−9 resolved peaks in the aliphatic region. In contrast, the hydrated elastin spectrum is typically characterized by a weaker and broader backbone carbonyl, with fewer peaks in the aliphatic region. Most pronounced are the $^{13}C\alpha$-Ala peak at 53 ppm and upfield methyl groups. The resolved aliphatic peaks are also characterized by narrow line widths not typically seen in proteins in the solid state. It is noted that the heteroaromatic cross-linking moieties, desmosine and isodesmosine, are not observed in natural-abundance ^{13}C NMR spectra due to their low amounts.[27] In addition, the relaxation behavior of the lyophilized elastin is typical for a solid-phase protein, whereas much of the wet protein is characterized by shorter time constants, reflecting a significant degree of motion.

The line widths obtained from the indirect dimension of the dipolar WISE 2D spectrum experiment are interpreted as indicators of relative mobility; i.e., more rigid domains have broader line shapes, and narrower peaks reflect faster motion. With ^{13}C decoupling applied during the t_1 evolution period, the line widths are presumed to be reflective of ^{1}H homonuclear dipolar couplings and, hence, interpreted as a quantitative indicator of mobility.

The contour plot of the 2D WISE spectrum acquired for lyophilized elastin is shown in Figure 1. These assignments are based on previous studies of elastin[4,6,7,28] and aggregate data in the Biological Magnetic Resonance Data Bank.[29] ^{1}H line shapes for each of the resolved ^{13}C sites in the aliphatic envelope are illustrated in Figure 2. All of them have several sets of spinning sidebands, as expected.

Our initial analysis of the line shapes in the indirect dimension was based on the assumption that there was only one population in the sample. However, this scenario is not likely, as the single-component MAS spectrum proved to be only a good first approximation. Instead, the better fits were obtained using two components. Representative line-fitting results are illustrated in Figure 3. Clearly, the +1 and −1 sidebands of the single-component spinning sideband pattern (Figure 3a) have greater intensities than observed experimentally. Two basic types of the two-component fits were then considered. One is a broad pattern with spinning sidebands, in addition to a single peak at the center frequency (Figure 3b), such as used with the onion cell wall material in

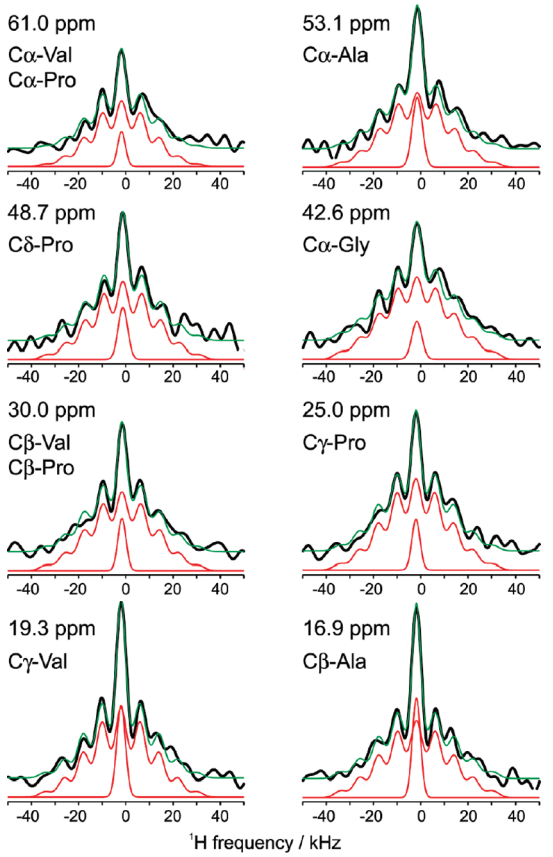

Figure 2. ^{1}H line shapes for each of the resolved ^{13}C sites in lyophilized elastin with 1 ms contact time and 8 kHz MAS (black lines). Individual components and the sum of the two-component model ($S(\omega) = S_1(\omega) + S_2(\omega)$) are shown in red and green, respectively.

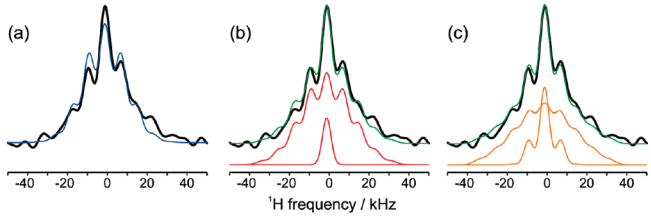

Figure 3. Fits of the ^{1}H slice corresponding to carbonyl peak (173.3 ppm) using a (a) single-component fit ($S(\omega) = S_1(\omega)$, blue line) and two-component fits with (b) broad and narrow line shapes ($S(\omega) = S_1(\omega) + S_2(\omega)$, red lines) and (c) two spinning sideband patterns ($S(\omega) = S_1(\omega) + S_1'(\omega)$, orange lines). Green lines indicate the sum of individual components for each two-component model. The rmsd values between the observed and calculated slices are 0.039, 0.029, and 0.027 for (a), (b), and (c), respectively.

an earlier study.[21] Alternatively, one might use two overlapping spinning sideband patterns of varying intensities and widths (Figure 3c).

An rmsd value was calculated for each simulated spectrum to quantify the goodness of its fit to the experimental data. Smaller rmsds reflect a better match and fewer differences. Regarding Figure 3, for example, the rmsd for the single-component pattern of spinning sidebands with one center frequency is 0.039, in contrast to the line shapes describing two populations (rmsd ~ 0.029 and 0.027). The 2-fold distributions appeared equally likely at this stage.

The results of the fits for the two-component pattern (S_1, S_2), described as one broad pattern with sidebands and one narrow (single) peak, are summarized in Table 1. The width of the broad component is 29.6−34.4 kHz. With the low

Table 1. Fits of the ^{1}H Line Shapes for Lyophilized Elastin with 1 ms Contact Time According to the Two-Component Model ($S(\omega) = S_1(\omega) + S_2(\omega)$)

ppm	assignment	I_1[a]	Δ_1/kHz	λ_1/kHz[b]	I_2[a]	Δ_2/kHz	S_2/S_1[c]
173.3	C=O	0.58	29.9 ± 0.6	7.1	0.31	5.1 ± 0.5	0.092
61.0	Pro Cα, Val Cα	0.36	29.6 ± 0.9	6.3	0.19	3.9 ± 0.5	0.072
53.1	Ala Cα	0.40	32.5 ± 0.9	6.6	0.39	5.0 ± 0.4	0.149
48.7	Pro Cδ	0.43	32.0 ± 1.0	6.3	0.29	4.7 ± 0.5	0.100
42.6	Gly Cα	0.44	34.4 ± 0.9	6.8	0.21	4.9 ± 0.7	0.068
30.0	Pro Cβ, Val Cβ	0.43	32.6 ± 0.8	6.5	0.29	4.0 ± 0.4	0.084
25.0	Pro Cγ	0.50	32.4 ± 0.6	6.5	0.28	4.0 ± 0.3	0.070
19.3	Val Cγ	0.49	32.0 ± 0.8	6.1	0.51	4.4 ± 0.2	0.142
16.9	Ala Cβ	0.42	34.4 ± 0.8	6.3	0.56	4.1 ± 0.2	0.156

[a] Fitting errors of I_1 and I_2 are within 0.01−0.02 and 0.02−0.03, respectively. [b] Fitting error of λ_1 is within 0.1−0.2 kHz. [c] $S_2/S_1 = (\Delta_2 I_2)/(\Delta_1 I_1)$.

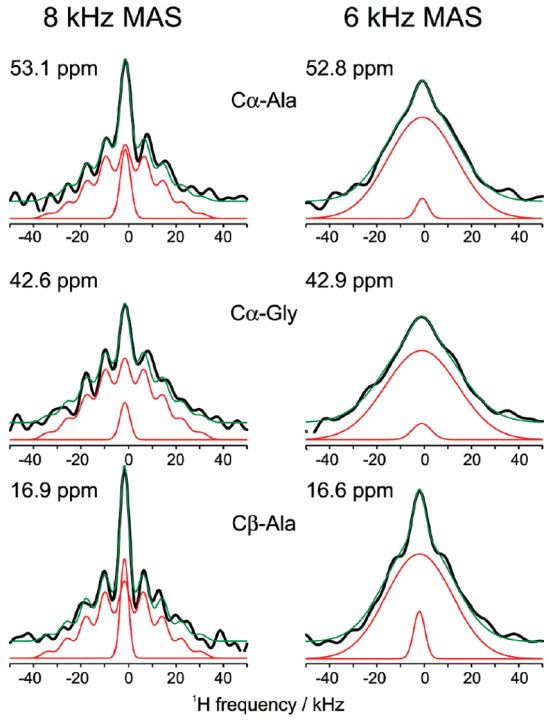

Figure 4. Comparison of the ^{1}H line shapes at 8 kHz (left) and 6 kHz (right) (black lines). In both experiments, 1 ms contact time was applied. Individual components for fits with two-component model ($S(\omega) = S_1(\omega) + S_2(\omega)$ for 8 kHz and two Gaussian line shapes for 6 kHz) are shown in red. The sum of the components is shown in green.

uncertainties (≤1 kHz), the similarities are more apparent than the differences. The line widths of the narrow component are also relatively uniform across the sample. They are roughly 1 order of magnitude smaller, with values of 3.9−5.1 kHz.

The sum of one narrow and one broad pattern became the more likely scenario after the WISE experiment was run at a slower spin rate. In Figure 3, the simulated pattern with two broad components, i.e., two sideband patterns, fit the experimental line shape as well as the sum of a one sideband pattern plus the (single) centerband peak. However, if the better model for the dynamics consisted of two rigid populations, each with its own set of spinning sidebands and comparable widths, then the change observed upon decrease of spin rate would likely differ from that of a narrow (mobile) peak plus one spinning sideband pattern (rigid). Figure 4 illustrates representative slices from WISE spectra obtained with 8 and 6 kHz sample spinning rates, whereby the latter falls into the "slow spinning regime".[11] The spinning sidebands are not apparent at the slower spinning speed. When the slices are fit with the two-component model utilizing a single narrow peak and a broader distribution with spinning sidebands, the width of the former does not differ significantly from the 8 kHz data, leading us to conclude that this scenario is more likely than the one with two spinning sideband patterns; i.e., if the proton line shape were comprised of two overlapping spinning sideband patterns, then the overall widths of both should have increased at slower spin rates, which is not the case here.

The broad and narrow peaks are present in varying proportion for the various resolved sites, as shown by the calculated ratio S_2/S_1, included in Table 1. The signal intensity ratios for the Cα carbons (except Cα-Gly) range from 0.072 to 0.149, whereas the Cα-Gly ratio of 0.068 is slightly lower. This result indicates that the proportion of the mobile backbone component is relatively uniform across the sample, although slightly more of the rigid fraction is populated in the Gly-rich regions. Finally, the ratios are highest in the methyl peaks at ∼0.156.

Previously published results of similar experiments on related proteins and peptides provided order parameters for resolved sites.[20,30] To obtain the order parameters, the dipolar couplings were obtained for related model compounds at the "rigid limit". Analogously, WISE data were collected for the single amino acids Gly, Ala, and Val, as shown in Table 2.

Glycine has broader line shapes in the indirect dimension, as compared to the result for the elastin. For the single amino acid, both carbonyl and Cα carbons are fit with the two-component line shape, i.e., narrow and broad. However, the line widths of the broad components of the upfield and downfield carbons are 42.9 and 40.7 kHz, respectively. Thus, the glycines in elastin have order parameters of ∼0.8. In addition, the single amino acid's indirect dimension line shapes have different ratios of narrow-to-broad, as compared to elastin, $S_2/S_1 = 0.055$ and 0.039 for the carbonyl and Cα, as compared to 0.092 and 0.068 in elastin. The ratios in the elastin are ∼1.7 times higher than found in the single amino acid, providing additional support for the "goodness" of these numbers, as they reflect mobility in the backbone of elastin in a consistent manner. More importantly, these values can be used to again conclude that mobility in the Gly-rich hydrophobic domains of elastin is higher than found in the single amino acid type.

Valines are also found almost exclusively in the hydrophobic domains of elastin. When the elastin WISE data are compared with those of the valine sample, a similar result is found. Again, a two-component fit is best. The broad components corresponding to the five valine carbons are nearly uniform (33−34 kHz), as are the narrow contributions (∼4 kHz). The ratios S_2/S_1 are ∼0.07−0.08, higher than that observed for glycine. Presumably, the higher mobile fraction is due to the presence of the two methyl groups on each valine. These values are compared to the elastin spectra, and the order parameters of 0.88 are calculated for both carbons on the backbone. The side-chain carbons Cβ and the

Table 2. Fits of the ^{1}H Line Shapes for the Amino Acids with 1 ms Contact Time According to the Two-Component Model ($S(\omega) = S_1(\omega) + S_2(\omega)$)

amino acid	ppm	assignment	I_1[a]	Δ_1/kHz	λ_1/kHz[b]	I_2[a]	Δ_2/kHz	S_2/S_1[c]
Gly	174.4	C=O	0.57	40.7 ± 0.5	8.0	0.35	3.6 ± 0.2	0.055
	42.4[d]	CαH$_2$	0.48	42.9 ± 0.5		0.28	2.8 ± 0.2	0.039
L-Val	175.7	C=O	0.37	34.1 ± 0.5	7.3	0.21	4.2 ± 0.3	0.069
	61.4	CαH	0.37	33.5 ± 0.4	7.4	0.21	3.8 ± 0.2	0.065
	31.0	CβH	0.35	33.0 ± 0.4	7.5	0.20	3.9 ± 0.2	0.066
	21.8	CγH$_3$	0.46	33.0 ± 0.3	7.4	0.33	3.5 ± 0.1	0.077
	19.3	CγH$_3$	0.55	33.1 ± 0.3	7.5	0.40	3.5 ± 0.1	0.074
L-Ala	177.6	C=O	0.45	31.5 ± 0.3	7.2	0.36	4.2 ± 0.1	0.106
	50.9	CαH	0.40	31.3 ± 0.3	7.0	0.35	3.5 ± 0.1	0.098
	20.3	CβH$_3$	0.49	30.0 ± 0.4	7.4	0.48	3.3 ± 0.1	0.107

[a] Fitting errors of I_1 and I_2 are below −0.01 and within 0.01−0.02, respectively. [b] Fitting error of λ_1 is within 0.1−0.2 kHz. [c] $S_2/S_1 = (\Delta_2 I_2)/(\Delta_1 I_1)$. [d] Two Gaussian line shapes were used to fit the result.

Cγ methyl carbons have slightly higher order parameters, approaching unity. Presumably, the "sticky", buried methyl groups may impede the motion of the backbone to some extent, resulting in order parameters that are less than 1, but not as mobile as the Gly-containing regions. We note that the S_2/S_1 ratios for the valines in elastin appear to be unchanged at first glimpse. However, these natural-abundance elastin spectra are somewhat complicated by the overlap of, particularly, the Val and Pro carbons. The Pro measurements (not shown) are complicated by what appears to be fast motion, so it is difficult to make further conclusions about the overlapping Val resonances.

Finally, the order parameters for the likely peaks of Ala in elastin are calculated with the values obtained from the measurement of the single amino acid. Ala is found in both cross-linking and hydrophobic domains. On its own, the carbons of alanine show good agreement with each other, as they did for both valine and glycine; i.e., the line widths of the broad and narrow components are 30−31.5 kHz (± 1%) and 3.3−4.2 kHz (±0.3%), with S_2/S_1 ratios of ∼0.10−0.11. The order parameters now slightly exceed unity, indicating that the protein's Ala carbons exhibit less mobility than in the free amino acid. In addition, the Cα and Cβ carbons have S_2/S_1 ratios of 0.15 and 0.16, indicating that the mobile component is higher in Ala-rich domains, although perhaps to a lesser extent than found in the Gly- and Val-rich hydrophobic regions.

The comparisons with the single amino acids and the elastin are summarized in Figure 5. Here, the Gly, Val, and Ala are shown with the order parameters calculated for the respective sites in elastin. The hydrophobic domains are characterized by the abundant Gly residues. Nearly all valines are found in these domain types as well. Hence, these WISE measurements indicate that there is more motion along the backbone in the hydrophobic domains. Less or no motion is observed in the hydrophobic side chains. Rigidity also appears to be characteristic for the cross-linking domains.

2. Shorter CP Time Used To "Filter" Directly Bound ^{13}C−^{1}H Spin Pairs. The magnetization transfer in Hartmann−Hahn cross-polarization occurs via the ^{13}C−^{1}H dipolar couplings, so short CP times can be used to select the directly bound ^{13}C−^{1}H spin pairs, such as in methine (CH) and methylene (CH$_2$) groups.[31] This rate dependence was used in a related NMR study of elastin,[22] in which CP times were used to distinguish inter- and intramolecular couplings. In the HETCOR study, it was also determined that the CP dynamics were reasonably well-described by the more exacting treatment presented by Baldus and co-workers.[32] Such consistency is reasonable, as shorter CP times leave less time for spin diffusion and the consequent equilibration of spin temperature. Thus, a 200 μs contact time is a reasonably robust selection tool, or "filter", for the methine and methylene groups, as the methyl

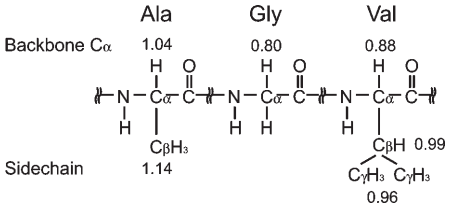

Figure 5. Order parameters S_{HH} for the resolved Ala, Gly, and Val backbone and side-chain carbons in elastin. S_{HH} values are calculated for data acquired with 1 ms CP time. The values are not significantly changed with a 200 μs CP time.

and nonprotonated carbons are only very weakly polarized, if at all. Figure 6 gives representative spectra obtained with a 200 μs contact time, in contrast to the 1 ms CP time used in previous figures. The relative contribution from the narrow components to total line shapes corresponding to Cα-Ala, Cδ-Pro, and Cβ-Pro/Val is significantly reduced, with S_2/S_1 ratios decreased from 0.149 to 0.079, 0.100 to 0.037, and 0.084 to 0.037, respectively (Table 3). In contrast, the S_2/S_1 ratios for the methyl and backbone carbonyl carbons are not changed significantly.

An interesting point is noted for the methylene groups for Cδ-Pro (48.6 ppm) and Cγ-Pro (24.7 ppm), as compared to Cα-Gly (43.0 ppm). The line shape of the methylene groups of Pro is the same with both CP times, i.e., the narrow peak coadded to the broader spinning sideband pattern. Most likely, the intramolecular motions of the ring puckering in proline residues[20,33] give rise to the narrow, mobile feature. In contrast, the Cα-Gly pattern with the 200 μs CP time has a markedly different appearance and lacks the "narrow peak". For this glycine line shape, the best fit is made with two spinning sideband patterns separated by a dipolar coupling of ca. 19 kHz, consistent with the ^{1}H−^{1}H distance in crystallographic data of α-glycine (1.77 Å, 21.7 kHz).[34] As noted above, ^{13}C decoupling is applied during t_1, so that the influence of the heteronuclear dipolar couplings can be ignored on the ^{1}H line shapes. Thus, we conclude that the separation comes from the homonuclear (^{1}H) local field effect. Dynamics similar to the ring pucker of the Pro are not expected here, as Cα-Gly is located in the backbone. A similar case of ^{1}H line shapes of methylene carbons with different mobilities was previously reported in a WISE study of the side-chain group of polysiloxane.[35]

3. Hydration of Elastin Results in the Nearly Uniform Narrowing of ^{1}H Line Shapes. The contour plot of the 2D WISE spectrum acquired for hydrated elastin is shown in Figure 7. Upon hydration, the ^{1}H line shapes collapse into narrow line shapes. In addition, it is noted that the ^{1}H line shapes do not give any appreciable sideband patterns, consistent with the conclusion that the protein undergoes rapid motions when fully hydrated.[6] Figure 8 gives representative

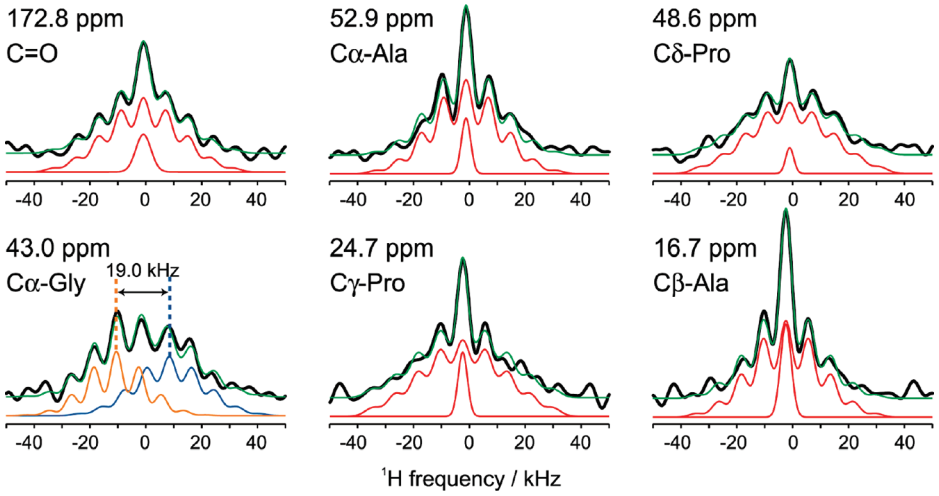

Figure 6. ^{1}H slices taken at specified ^{13}C sites in lyophilized elastin with 200 μs contact time and 8 kHz MAS (black lines). All line shapes except for Cα-Gly were fit with the two-component model ($S(\omega) = S_1(\omega) + S_2(\omega)$, red lines for individual components). Two spinning sideband patterns with the different center frequencies were used to fit Cα-Gly ($S(\omega) = S_1(\omega) + S_1'(\omega)$, blue and orange lines). Green lines indicate $S(\omega)$ for each two-component model.

Table 3. Fits of the ^{1}H Line Shapes for Lyophilized Elastin with 200 μs Contact Time According to the Two-Component Model ($S(\omega) = S_1(\omega) + S_2(\omega)$)

ppm	assignment	I_1[a]	Δ_1/kHz	λ_1/kHz[b]	I_2[a]	Δ_2/kHz	S_2/S_1[c]
172.8	C=O	0.35	31.2 ± 0.7	6.4	0.18	6.4 ± 0.6	0.107
60.1	Pro Cα, Val Cα	0.32	28.8 ± 1.0	6.1	0.17	4.6 ± 0.6	0.085
52.9	Ala Cα	0.44	29.3 ± 0.6	6.1	0.26	3.9 ± 0.3	0.079
48.6	Pro Cδ	0.32	35.0 ± 0.8	7.0	0.12	3.4 ± 0.6	0.037
43.0[d]	Gly Cα	0.28	29.2 ± 1.0	6.3			0.925[f]
43.0[e]	Gly Cα	0.31	25.2 ± 0.9	5.4			
30.1	Pro Cβ, Val Cβ	0.39	34.5 ± 0.7	6.0	0.14	3.4 ± 0.5	0.037
24.7	Pro Cγ	0.35	36.5 ± 0.8	6.9	0.31	3.9 ± 0.3	0.094
19.3	Val Cγ	0.48	29.6 ± 0.7	5.7	0.52	4.4 ± 0.2	0.158
16.7	Ala Cβ	0.46	29.5 ± 0.7	5.9	0.44	4.5 ± 0.2	0.150

[a] Fitting errors of I_1 and I_2 are below −0.01 and within 0.01−0.02, respectively. [b] Fitting error of λ_1 is within 0.1−0.2 kHz. [c] $S_2/S_1 = (\Delta_2 I_2)/(\Delta_1 I_1)$. [d,e] Fit of Gly Cα requires two spinning sideband patterns [d]S1(ω), [e]S1′ (ω) that are separated by ~19 kHz. [f] $S_1'/S_1 = (\Delta_1' I_1')/(\Delta_1 I_1)$ is used for the fit of Gly Cα.

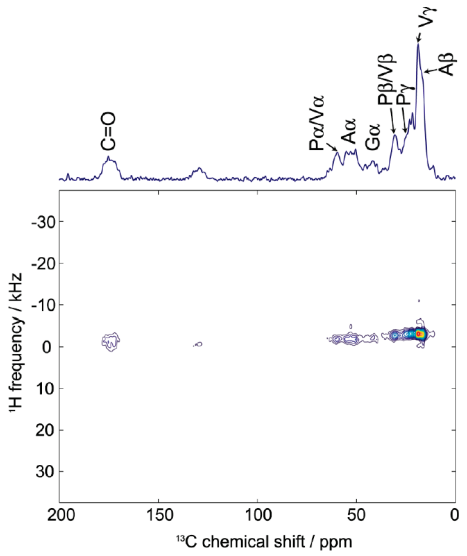

Figure 7. ^{1}H−^{13}C 2D WISE spectrum of hydrated elastin with 1 ms contact time and 8 kHz MAS. Skyline projection along the ^{13}C dimension is also shown.

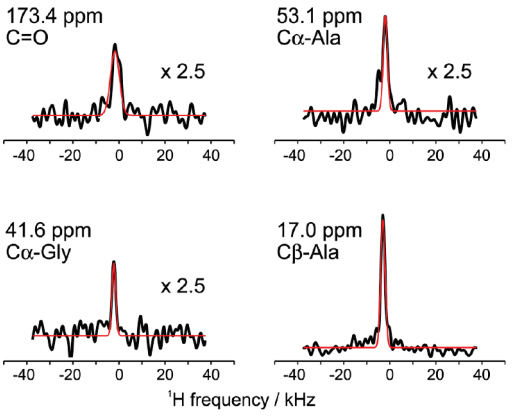

Figure 8. Representative ^{1}H line shapes of hydrated elastin with 1 ms contact time and 8 kHz MAS. Fits with single Gaussian line shape ($S(\omega) = S_2(\omega)$) are shown in red. Slices for the backbone carbons are magnified along the vertical direction.

data, as obtained for the backbone carbonyl, Cα-Ala, Cα-Gly, and Cβ-Ala carbons.

Our recent study of hydrated elastin by ^{1}H−^{13}C HETCOR spectroscopy[22] indicates that 1 ms CP time mainly reflects the ^{1}H−^{13}C heteronuclear dipolar couplings in the directly bonded spin pairs. Motion is fast enough that cross-peaks due to interstrand correlations are diminished. Hence, ^{1}H line shapes observed here reflect an almost uniform, fast motion for each resolved carbon peak.

Table 4 summarizes the information obtained for the line shapes of the indirect dimension. Nearly all peaks correlated with aliphatic carbons have widths $\Delta \sim 1.8$−2.3 kHz.

Table 4. Fits of the ^{1}H Line Shapes for Hydrated Elastin with Single Gaussian Line Shape

ppm	assignment	I	Δ/kHz
173.4	C═O	0.15 ± 0.01	4.5 ± 0.2
60.7	Pro Cα, Val Cα	0.20 ± 0.01	1.9 ± 0.1
53.1	Ala Cα	0.22 ± 0.01	2.2 ± 0.1
41.6	Gly Cα	0.17 ± 0.01	1.9 ± 0.1
30.8	Pro Cβ, Val Cβ	0.34 ± 0.01	2.2 ± 0.1
25.3	Pro Cγ	0.32 ± 0.01	2.3 ± 0.1
19.0	Val Cγ	1.00 ± 0.02	1.8 ± 0.1
17.0	Ala Cβ	0.74 ± 0.02	2.3 ± 0.1

The backbone carbonyls give the broadest proton line shape of $\Delta = 4.5$ kHz. The asymmetric, non-Gaussian line shape of the backbone carbonyl site is noted, most likely due to the ^{1}H chemical shift dispersion that becomes apparent with the diminishing natural line widths. There are no bonded protons on the backbone carbonyl carbons; thus, the observation of the C═O peak indicates the dipolar interaction among ^{13}C═O and neighboring nonbonded protons during CP, most likely Hα and HN. In fact, a symmetric line shape was observed in the WISE experiment in D_2O (data not shown), probably due to the effect of NH/ND exchange. Hence, the asymmetric line shape may reflect the chemical shift difference between those protons. These line widths are all well below those typically observed in the solid state for rigid polymers.

Conclusion

The WISE experiment provides yet more evidence that elastin has a unique dynamic profile. Comparison of its ^{1}H line shapes are made with similar systems, such as natural rubber and elastic biopolymers.

Elastin's narrow lines are similar in some respects to those reported for natural rubbers. WISE experiments on a series of vulcanized rubbers similarly yielded a two-component line shape, dubbed "mobile" (for the narrow) and "rigid" (for broader pattern).[15] Generally, the former yielded line widths over the range of 0.9−1.9 kHz, whereas the latter displayed widths of 1.5−7.5 kHz. In contrast, elastin is most mobile when fully hydrated, although its widths (~2 kHz), particularly for the aliphatic carbons, are slightly broader than that observed for the rubber. Possibly, the degree of motional narrowing observed in the case of the rubbers is not exactly mimicked in elastin. Note that the 2-fold nature of elastin's dynamics is reported here only for the brittle, lyophilized elastin, not the elastic, hydrated state. It should be reiterated that there is a considerable segment of the protein that does not cross-polarize, i.e., that we see only a portion (albeit a large one) of the entire protein. Hence, the overall signal intensity is lessened. If there are rigid and mobile domains in the hydrated elastin, the relative amount of the former may be significantly less than observed in the lyophilized state. Thus, the issues of relative sensitivity (total signal from CP) and broad line shapes (thus distributing an already small intensity over a broad frequency range) may preclude observation of a rigid component.

The studies of the spider silks provide additional insights. Holland and co-workers conducted WISE experiments on samples of silks from *Nephila clavipes*.[17] The dragline silk consists of two major ampullate silk proteins that have alternating poly(Ala) and Gly-rich regions.[36,37] The polyalanine regions in spider silk bear some resemblance to the Ala-rich cross-linking domains of elastin. In addition to the similarities in composition, spider silk is an immediately relevant system, as it is elastic when in its supercontracted state; i.e., upon hydration, the dragline silk fiber undergoes decreases in strength and stiffness and an increase in elasticity.[38,39] ^{1}H slices in the WISE spectrum of the dry dragline silk were characterized by a single broad feature (width ~ 40 kHz), in contrast with the two-component line shapes in lyophilized elastin observed with the 1 ms CP time. The narrow component, likely representing a more mobile fraction, is present in elastin, even in the absence of water. The width of the dry silk is roughly equivalent to that of the broader component in lyophilized elastin, probably reflecting a general characteristic of dehydrated proteins. In addition to the differences in the overall line shapes, the ^{1}H slice corresponding to β-sheetlike Cβ-Ala in silk has a broad component, even in the hydrated state. This result was interpreted as evidence for the nonpermeability of water into the crystalline β-sheet region of spider silk. In contrast, none of the broad spinning sideband patterns are retained with hydration of elastin. If a similar logic is applied here, then this WISE result shows that water permeates the entirety of elastin and, likely, the elastic fiber.

Finally, the results of this dipolar WISE experiment on the native elastin may be compared with those of the related LG-WISE work on the repeating polypentapeptide mimetic of elastin.[20] It is also noted that this mimetic is soluble in water, so it was only hydrated to 30 wt % water, whereas the fully hydrated elastin is ~60−80% water and does not dissolve. In addition, the mimetic was not cross-linked. The results are qualitatively similar to those in this study; namely, broad components in the dry state collapse to narrow components in the partially hydrated state. However, their results differ quantitatively, with widths of 58−67 kHz for the dry state (except Cγ-Val, 28 kHz) and 12.5 kHz for the partially hydrated peptide (except Cα-Gly, 7.8 and 29 kHz). Here it is noted that the line widths of the indirect dimension were interpreted as reflective of ^{1}H−^{1}H dipolar couplings, although ^{13}C decoupling during t_1 was not applied. Hence, their results likely reflect both ^{1}H−^{1}H and ^{1}H−^{13}C dipolar couplings.[35] Another substantive difference is the lack of a 2-fold dynamics in the dry state; i.e., the line shape does not appear at all similar to the two-component line shapes observed in the native state. Finally, the order parameters differ somewhat for the native elastin and the mimetic. The order parameters for the completely dehydrated elastin mimetic were obtained with ^{1}H−^{13}C couplings from the LG-CP experiment. Although differing slightly from our approach, the basic trends in peptide dynamics can still be compared. In the mimetic, the order parameters S_{CH} in the mimetic approached unity for all of the backbone Cα. Side chains in the mimetic displayed more mobility. In contrast, the native elastin shows more mobility in the Cα sites in both Gly and Val, the predominant amino acids in the hydrophobic domains, as compared to the single amino acids. Furthermore, the side chains of native elastin's hydrophobic domains appear to be less mobile than those of the mimetic. Line shapes of both mimetic and native protein collapse nearly uniformly upon hydration, although the variation is slightly higher in the latter. It appears that the elastin peptide based solely on its hydrophobic domains does not exactly mimic the local dynamics present in the native protein.

One might ask if the origin of the narrow features in the indirect dimension of hydrated elastin is H_2O interacting with elastin. However, this scenario is unlikely, based on two observations. First, the dispersion of ^{1}H chemical shifts was observed, and it was consistent with the result of ^{1}H−^{13}C HETCOR.[22] If water−protein interactions were the major source of the mobile population, then narrow peaks would be observed at the water frequency in the indirect dimension.[40] However, the telltale cross-peaks were not observed. Additional evidence was obtained from the WISE experiment of elastin in D_2O, which showed the narrow components in the indirect dimension (data not shown). Again, if H_2O molecules were the origin of the narrow components, then the use of D_2O would suppress the signals in the WISE data. However, the signal intensities from elastin after D_2O exchange

were comparable to those reported herein. Hence, the origin of the narrow components is most likely attributed to the fast mobility in hydrated elastin.

Overall, this study demonstrates that WISE and other two-dimensional experiments may be used to extract dynamic profiles for the resolved sites in samples of unenriched elastin. These results show that the dynamic heterogeneity in native, hydrated elastin is somewhat mirrored in samples in which the water is removed; i.e., even in the absence of the plasticizing water, the rigid and mobile segments in elastin retain such identities. Furthermore, it confirms our earlier experiments that the presence of water effects increased mobility across the entire protein, unlike what was reported for supercontracted spider silk. It does appear that elastin's dynamic profile is unique, mirroring some aspects of natural rubber in addition to features of an elastic morphology of spider silk. As such, the best model for elastin's structure−function likely shares features with these systems, such as the interleaved mobile and rigid domains, with its unique composition and yet-to-be determined structural makeup providing additional definition.

Acknowledgment. This work was partially supported by a grant to KKK from the National Science Foundation (MCB-0344975). The authors also thank an anonymous reviewer for the suggestion to use the single amino acids to obtain the "rigid limit" values and consequent order parameters for the analysis.

References and Notes

(1) Rosenbloom, J.; Abrams, W. R.; Mecham, R. *FASEB J.* **1993**, *7*, 1208–1218.
(2) Mithieux, S. M.; Weiss, A. S. *Adv. Protein Chem.* **2005**, *70*, 437–461.
(3) Torchia, D. A.; Piez, K. A. *J. Mol. Biol.* **1973**, *76*, 419–424.
(4) Kricheldorf, H. R.; Muller, D. *Int. J. Biol. Macromol.* **1984**, *6*, 145–151.
(5) Perry, A.; Stypa, M. P.; Foster, J. A.; Kumashiro, K. K. *J. Am. Chem. Soc.* **2002**, *124*, 6832–6833.
(6) Perry, A.; Stypa, M. P.; Tenn, B. K.; Kumashiro, K. K. *Biophys. J.* **2002**, *82*, 1086–1095.
(7) Pometun, M. S.; Chekmenev, E. Y.; Wittebort, R. J. *J. Biol. Chem.* **2004**, *279*, 7982–7987.
(8) Hoeve, C. A. J.; Flory, P. J. *Biopolymers* **1974**, *13*, 677–686.
(9) Gosline, J. M. *Symp. Soc. Exp. Biol.* **1980**, *34*, 332–357.
(10) Debelle, L.; Tamburro, A. M. *Int. J. Biochem. Cell Biol.* **1999**, *31*, 261−272 and references therein.
(11) Schmidt-Rohr, K.; Clauss, J.; Spiess, H. W. *Macromolecules* **1992**, *25*, 3273–3277.
(12) Clauss, J.; Schmidt-Rohr, K.; Adam, A.; Boeffel, C.; Spiess, H. W. *Macromolecules* **1992**, *25*, 5208–5214.
(13) Tekely, P.; Palmas, P.; Mutzenhardt, P. *Macromolecules* **1993**, *26*, 7363–7365.
(14) Eulry, V.; Tekely, P.; Humbert, F.; Canet, D.; Marcilloux, J. *Polymer* **2000**, *41*, 3405–3410.
(15) Malveau, C.; Tekely, P.; Canet, D. *Solid State Nucl. Magn. Reson.* **1997**, *7*, 271–280.
(16) Holland, G. P.; Jenkins, J. E.; Creager, M. S.; Lewis, R. V.; Yarger, J. L. *Biomacromolecules* **2008**, *9*, 651–657.
(17) Holland, G. P.; Lewis, R. V.; Yarger, J. L. *J. Am. Chem. Soc.* **2004**, *126*, 5867–5872.
(18) Caravatti, P.; Bodenhausen, G.; Ernst, R. R. *Chem. Phys. Lett.* **1982**, *89*, 363–367.
(19) van Rossum, B. J.; de Groot, C. P.; Ladizhansky, V.; Vega, S.; de Groot, H. J. M. *J. Am. Chem. Soc.* **2000**, *122*, 3465–3472.
(20) Yao, X. L.; Conticello, V. P.; Hong, M. *Magn. Reson. Chem.* **2004**, *42*, 267–275.
(21) Hediger, S.; Lesage, A.; Emsley, L. *Macromolecules* **2002**, *35*, 5078–5084.
(22) Ohgo, K.; Niemczura, W. P.; Kumashiro, K. K. *Macromolecules* **2009**, *42*, 7024–7030.
(23) Martin, S. L.; Vrhovski, B.; Weiss, A. S. *Gene* **1995**, *154*, 159–166.
(24) Martin, R. W.; Paulson, E. K.; Zilm, K. W. *Rev. Sci. Instrum.* **2003**, *74*, 3045–3061.
(25) Metz, G.; Wu, X. L.; Smith, S. O. *J. Magn. Reson., Ser. A* **1994**, *110*, 219–227.
(26) Bennett, A. E.; Rienstra, C. M.; Auger, M.; Lakshmi, K. V.; Griffin, R. G. *J. Chem. Phys.* **1995**, *103*, 6951–6958.
(27) Kumashiro, K. K.; Kim, M. S.; Kaczmarek, S. E.; Sandberg, L. B.; Boyd, C. D. *Biopolymers* **2001**, *59*, 266–275.
(28) Kumashiro, K. K.; Ho, J. P.; Niemczura, W. P.; Keeley, F. W. *J. Biol. Chem.* **2006**, *281*, 23757–23765.
(29) Ulrich, E. L.; Akutsu, H.; Doreleijers, J. F.; Harano, Y.; Ioannidis, Y. E.; Lin, J.; Livny, M.; Mading, S.; Maziuk, D.; Miller, Z.; Nakatani, E.; Schulte, C. F.; Tolmie, D. E.; Wenger, R. K.; Yao, H. Y.; Markley, J. L. *Nucleic Acids Res.* **2008**, *36*, D402–408.
(30) Reichert, D.; Pascui, O.; deAzevedo, E. R.; Bonagamba, T. J.; Arnold, K.; Huster, D. *Magn. Reson. Chem.* **2004**, *42*, 276–284.
(31) Wu, X.; Burns, S. T.; Zilm, K. W. *J. Magn. Reson., Ser. A* **1994**, *111*, 29–36.
(32) Lange, A.; Seidel, K.; Verdier, L.; Luca, S.; Baldus, M. *J. Am. Chem. Soc.* **2003**, *125*, 12640–12648.
(33) Sone, M.; Yoshimizu, H.; Kurosu, H.; Ando, I. *J. Mol. Struct.* **1993**, *301*, 227–230.
(34) Langan, P.; Mason, S. A.; Myles, D.; Schoenborn, B. P. *Acta Crystallogr.* **2002**, *B58*, 728–733.
(35) Palmas, P.; Tekely, P.; Canet, D. *Solid State Nucl. Magn. Reson.* **1995**, *4*, 105–111.
(36) Xu, M.; Lewis, R. V. *Proc. Natl. Acad. Sci. U.S.A.* **1990**, *87*, 7120–7124.
(37) Hinman, M. B.; Lewis, R. V. *J. Biol. Chem.* **1992**, *267*, 19320–19324.
(38) Shao, Z. Z.; Young, R. J.; Vollrath, F. *Int. J. Biol. Macromol.* **1999**, *24*, 295–300.
(39) Guinea, G. V.; Elices, M.; Perez-Rigueiro, J.; Plaza, G. R. *J. Exp. Biol.* **2005**, *208*, 25–30.
(40) Lesage, A.; Gardiennet, C.; Loquet, A.; Verel, R.; Pintacuda, G.; Emsley, L.; Meier, B. H.; Bockmann, A. *Angew. Chem., Int. Ed.* **2008**, *47*, 5851–5854.